

Overview on stationary and transient divertor heat loads

A. Herrmann

Max-Planck-Institut für Plasmaphysik, EURATOM Assoziation, D-85740-Garching, Germany

Abstract: The divertor concept and the divertor materials envisaged for ITER FEAT requires certain values for the maximum of the stationary and the transient heat flux. The maximum stationary heat flux is limited by the active cooling structure. The limit for transient events is given by the maximum tolerable surface temperature. This paper will review the efforts made to investigate and to understand the different possibilities of divertor heat flux reduction. Proper geometric orientation of the divertor targets reduces the parallel heat flux by a factor of 10 to 50. The radiation capability of closed divertor configuration is doubled compared to open configurations. A further reduction of maximum heat load can be achieved by increasing the wetted area in double null plasma configurations. Profile broadening depends on plasma parameters and is no independent parameter. The temporal and spatial distribution of the energy transported by strong edge localized modes (type I ELMs) is discussed.

1. Introduction

The power handling capacity of fusion experiments and fusion reactors is a crucial problem in using nuclear fusion for energy production. Whereas the power to be handled was a few kW for the first tokamaks, present tokamaks are running with a few ten MW heating power, and the next step device ITER is designed as a 500 MW experiment. This power has to be absorbed by components surrounding the plasma. There are three main channels of power loss: (i) Fusion neutrons and charge exchange (CX) particles, (ii) plasma radiation, (iii) convective and conductive heat transport. Whereas neutron, CX, and radiation losses are more or less isotropic, the heat conduction and convection is related to plasma ions and electrons, which are guided by the magnetic field lines. The heat flux along the first field line at the plasma edge is for present experiments in the order of a few hundred MW per square meter. A material interrupting a field line has to cope with this high heat flux.

The border between the region of closed magnetic field lines (plasma column) and field lines ending at materials (scrape off layer – SOL) is called separatrix. In early fusion experiments the separatrix was defined by a so called limiter, which has direct contact to the hot plasma. A decoupling of the plasma and the heat flux absorbing parts is achieved by special magnetic configurations which diverts the open field lines into a special part of the vacuum vessel – the divertor chamber. Such a divertor configuration was first realised at the Axial Symmetric Divertor EXperiment (ASDEX) in Garching [1]. The decoupling of heat absorbing components from the hot plasma column was a prerequisite for the achievement of the H-mode, a plasma with high energy confinement due to an improved transport barrier established at the plasma edge inside the separatrix.

H-mode scenarios with plasma shapes in divertor configurations are investigated at different experiments around the world and are the basis for the design of the next step experiment ITER. The objectives of divertor investigations are the particle handling for density control, alpha particle removal, and power handling.

This paper is focused on power handling problems in divertor configurations. The figures of merit of a divertor for the power handling capacity are discussed in chapter 2. Divertor evolution and geometric tools for heat flux mitigation are presented in chapter 3. The behaviour of averaged heat load to the divertor is investigated in chapter 4. Chapter 5 presents results from heat pulses which

causes a heat flux orders of magnitude higher than the averaged values. Finally, the results are summarised

It should be mentioned, that this paper is NO review about all experiments and theoretical activities at different fusion experiments around the world. The aim of this paper is to give an overview on the problems of heat flux deposition in divertors. It is based on published results.

2. Divertor design criteria

Upper limits for the heat flux onto the divertor surface are given by the properties of the target material and by the cooling capability of the divertor structure. Steady state experiments like ITER, Tore Supra, and the stellarator W7-X require an actively cooled target. Experiments with short pulse lengths are working with inertial cooling. The tolerable averaged stationary heat flux for actively cooled divertors is given by the amount of heat which can be removed by the cooling pipes. The design value for ITER and W7-X is $q_{\max} = 10 \text{ MW/m}^2$ [2,3]. The stationary surface temperature for this maximum load is about 1000 °C. For inertial cooled divertors the maximum heat flux is limited by the discharge duration, Δt , specific heat capacity of the absorbing target, ρc , the target thickness, d , and the maximum tolerable equilibrium temperature, ΔT_{eq} , which depends on construction details at the

clamping structure:
$$\Delta T_{eq} = \frac{q_s \Delta t}{d \rho c}.$$

The averaged heat flux for a carbon target with a heat capacity of $\rho c \approx 3 \text{ MWs/(m}^3 \text{K)}$, a target thickness of 30 mm thickness, a tolerable temperature increase $\Delta T_{eq} = 600 \text{ K}$, and 5 s pulse duration is about $q_{av} = 10 \text{ MW/m}^2$. This is a worst case estimation because it assumes a uniform heat load across the whole target surface.

Present discharge scenarios with high confinement are accompanied by heat bursts removing up to a few percent of the plasma stored energy on a 100 μ s time scale (see chapter 4). The deposition time of such events is short against the propagation time of the heat pulse through the target thickness which is in the order of seconds. This allows to derive the relation between heat flux and surface temperature from the solution of the 1D heat conduction equation for a semi-infinite target:

$$\Delta T_s^\infty(t) = \frac{2}{\sqrt{\rho b}} q_s \sqrt{\Delta t}$$

with: $b = \sqrt{\rho c}$; heat penetration coefficient $\left[\frac{\text{W}\sqrt{\text{s}}}{\text{m}^2 \text{K}} \right]$

The maximum tolerable temperature increase due to heat bursts is given by the stationary temperature increase and the tolerable surface temperature of the target material. From Equ. 1 follows that not the heat flux but the product of heat flux and square root of time is the parameter to be kept below a material dependent limit. The tolerable amount of energy deposited with a heat pulse increases with the square root of the deposition time.

The figures of merit for divertor heat flux judgement is a maximum value for the averaged heat flux of about 15 MW/m² and is a material dependent value for the energy impact, as shown in table 1 for graphite, carbon fibre composite (CFC), tungsten, and cooper.

material	heat conductivity $W / (m K)$	heat penetration coefficient $kW\sqrt{s} / (m^2 K)$	Temperature change K	energy impact $(MW\sqrt{s} / m^2)$
graphite (EK98)	49	13	1300	15
CFC (N11)	90	16	1300	18
tungsten	110	16	2400	38
cooper	390	37	600	19

3. Divertor geometry and heat flux mitigation

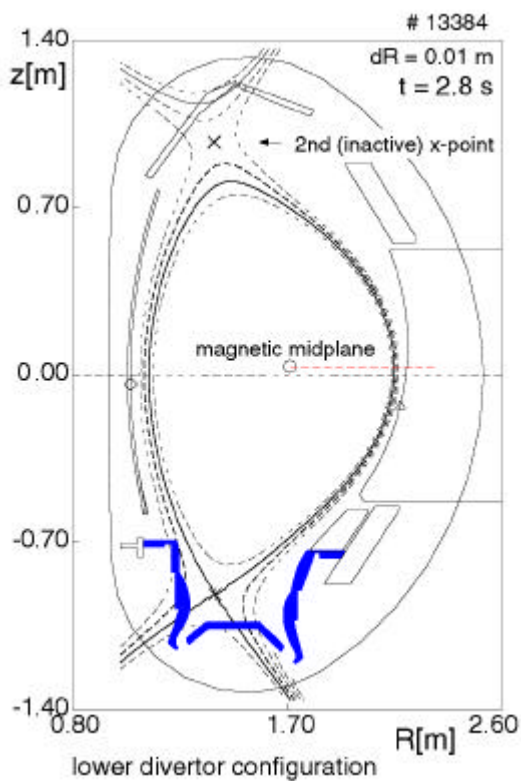


Figure 1. Magnetic configuration for a lower single null plasma configuration. The midplane distance of magnetic flux surfaces is 1 cm. The separatrix distance (active to inactive) is 1.5 cm in the midplane.

Power crossing the separatrix is transported by heat conduction and heat convection along magnetic field lines onto divertor plates. The contribution of geometry to mitigate the maximum heat flux at the divertor target is to make the area where the heat flux is deposited (wetted area) as large as possible. The magnetic configuration for a toroidally symmetric divertor (poloidal divertor) is produced by poloidal field coils. Such a magnetic configuration, as shown in Fig. 1, is characterised by the existence of the so called x-point – a singular point in the magnetic field configuration where the field lines are ergodic and infinitely long -, and two divertor legs. The lines in Fig. 1 are a cut through the areas of constant magnetic flux, whereas the distance between the lines is 1 cm in the magnetic midplane. The distance between areas of constant magnetic flux varies along the poloidal circumference of the plasma and becomes a maximum in the x-point region. This flux expansion offers a first possibility to reduce the maximum heat flux by selecting a position of the target plate where the flux expansion is high. The total power to the divertor can't be reduced this way. Typical values for the flux expansion at the location of the divertor plates are between 5 and 20.

Related to the flux expansion is the angle of inclination between the magnetic field lines and the

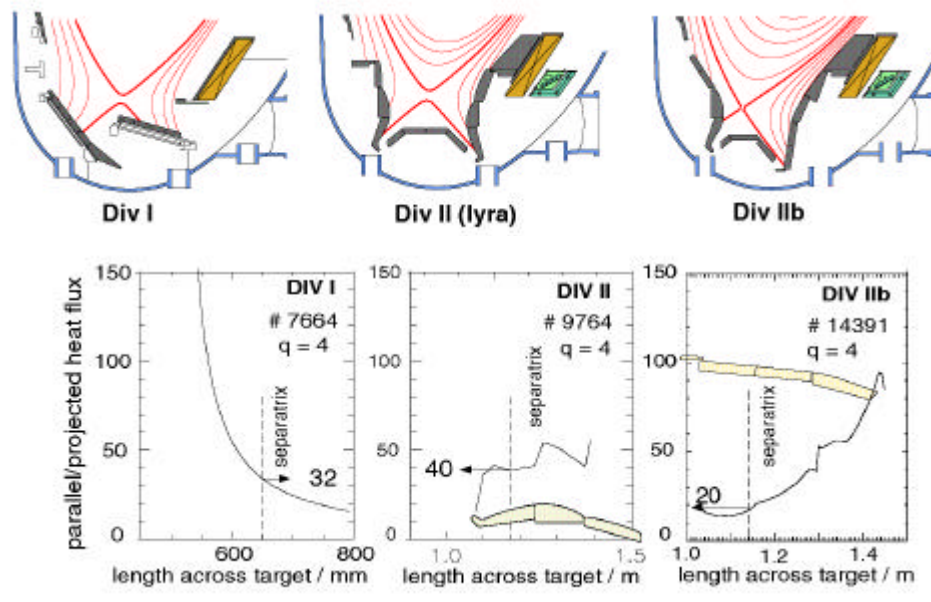


Figure 2. Divertor geometries investigated in ASDEX Upgrade (top) and corresponding pitch ratios (bottom).

target plate (pitch angle). This angle determines the pitch ratio, the ratio between the parallel heat flux transported along field lines and the projected heat flux loaded onto the target. The pitch angle

depends on the safety factor, i.e. the helicity of the magnetic field. It is nearly grazing at the target plate and increases to a few 10 degrees in the midplane. Due to the grazing incidence of the magnetic field lines at the divertor each toroidal gap between divertor plates results in a leading edge, i.e. a surface is hit nearly perpendicular by the magnetic field lines, the pitch ratio becomes about one and the surface is loaded with the parallel heat flux. As far as gaps between target plates are unavoidable leading edges are protected by tilting the target plates, so that the gaps itself are shadowed. But this tilting reduces the wetted area, typically by a few ten percent. This loss of wetted area can be avoided by minimising toroidal gaps.

Different divertor configurations used in ASDEX Upgrade and corresponding pitch factors are shown in Fig. 2. Div I is an open divertor with flat target plates not optimised for a special magnetic configuration and the pitch ratio varies strongly across the target plate. Div II is an optimised divertor as it is planned for ITER and was investigated at ASDEX Upgrade [4]. The geometric optimisation of the target shape results in a more or less smooth variation of the field line pitch across the strike point modules. But this optimised deep and nearly closed divertor works only for special plasma configurations. The increasing interest in plasma configurations with triangular shape which did not fit into the outer leg of Div II requires the installation of a less optimised but more flexible divertor

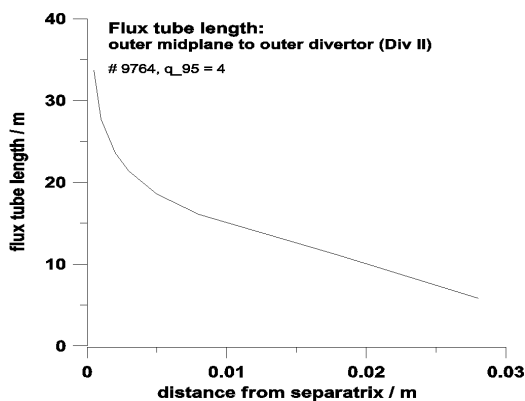


Figure 3. The length of the flux tube connecting outer midplane and outer divertor decreases with the distance from the separatrix.

(Div IIb) keeping the beneficial vertical position of the target plates. The corresponding pitch factor is more dynamic and more than a factor of 2 lower compared to the optimised divertor configuration.

A further geometric figure is a key element in the interpretation of the heat transport in the SOL. The flux tube length, the distance between the magnetic midplane and the target along field lines, determines the interaction region for particles and heat entering the midplane. The connection length as a function of the distance from the separatrix is shown in Fig. 3 for a magnetic configuration with a safety factor $q_{95} = 4$. The connection length is infinitely near the separatrix and decreases with the distance from it. With increasing q_{95} the connection length increases because of the decreasing helicity.

4. Stationary heat load

In this part we consider energy which escapes from the confinement region. It is transported by heat conduction and convection along a magnetic flux tubes to the divertor. On this way, energy can be lost from the flux tube by radial transport, by radiation and by charge exchange. This possible losses reduces the energy deposited directly to the target. The strength of the loss processes depends on the operational regime of the divertor.

In the case of a low density plasma with a high edge temperature the energy flow to the divertor is dominated by the parallel transport and is only limited by the capability of the electric sheath in front of the target to transfer the energy. The heat flux to the target is given by the ion flux, Γ_{ion} , the electron temperature in front of the sheath, T_e , and the sheath transmission factor, \mathbf{d} . It is about: $q_{||,mid} \approx q_{||,tar} = \mathbf{d} \Gamma_{ion} T_e$. The temperature ratio between midplane and divertor is about unity.

In this regime the separatrix density increases linearly with the neutral flux and the divertor density is about half the midplane separatrix density as expected for pressure balance (see. Fig. 4). The change from this low recycling divertor (or sheath limited regime) to a high recycling regime starts when the mean free path of neutrons attains the same order as the extend of the divertor region. Due to

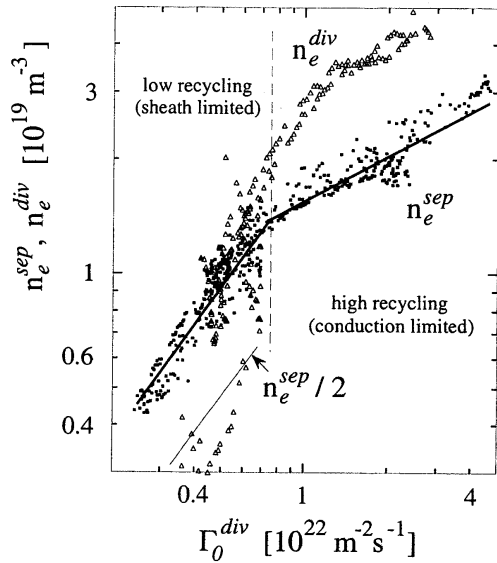


Figure 4. Dependence of the divertor and separatrix density on the neutral gas flux density for low and high recycling SOL-regime in ohmic discharges (ASDEX Upgrade).

the strong ionisation sources in front of the target, one gets a high density and a low electron temperature. The energy transport is now conduction limited. The electron heat conduction is the dominating process due to the higher mobility compared to the ions. The heat flux to the target is given by the temperature gradient along the flux tube and the electron heat conductivity, $k_0 T_e^{5/2}$, which strongly depends on the temperature:

$$q_{\parallel} = k_0 T_e^{5/2} \frac{\partial T_e}{\partial x}.$$

The heat flux profile at the midplane and that measured at the divertor plates are comparable for both regimes. The change from the sheath limited to the conduction limited regime happens at low densities so that the ASDEX Upgrade divertor operates in the conduction limited regime. A further increase of the density results first in a reduction of the energy flux to the target plates (partial detachment) due to increasing contributions of radiation and charge exchange. A significant broadening of the heat flux profile is found in the complete detached operation regime, when momentum loss becomes high.

4.1. Radiation capability

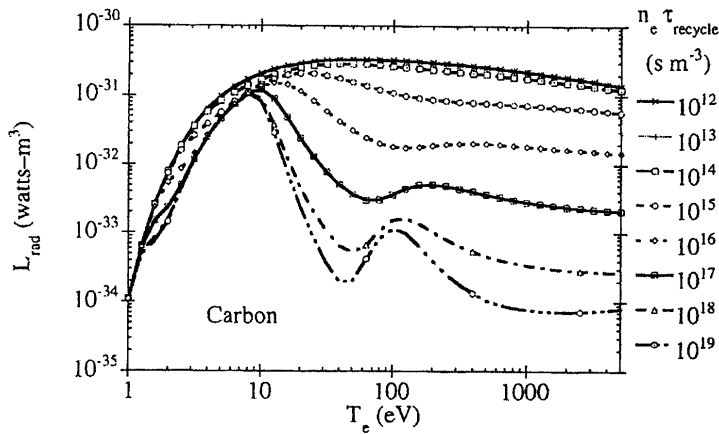


Figure 5. Radiation loss function for carbon as a function of electron temperature (D. Post).

strongly decreases at the low temperature part of the loss function. A further temperature reduction requires a radiator with a lower optimum temperature, such as hydrogen with a maximum of the radiation loss function at about 2 eV.

A high density of hydrogen and impurities is favourable for the radiation losses in the divertor region. But this high radiating regimes are mostly accompanied by a degradation of the energy confinement because an increase of edge density causes a decrease of edge temperature due to the edge pressure limit. In high confinement regimes with stiff temperature profiles this results in a decrease of the core temperature. This destructive effect of a high density in the divertor on the main plasma can be avoided by closing the divertor vs the main plasma as much as possible. The generation

The radiation capability along a field line depends on the ability to transfer particle energy into radiation energy. It can be estimated from the energy balance along field lines with a radiation loss rate, λ . Radiation loss functions for carbon are shown in Fig. 5. The residence time, t_{recycle} , is a measure for the distance from the coronal equilibrium. The short residence time of impurities close to the plate broadens the radiation loss function at the high temperature part and increases the total amount of radiative losses. Radiative losses

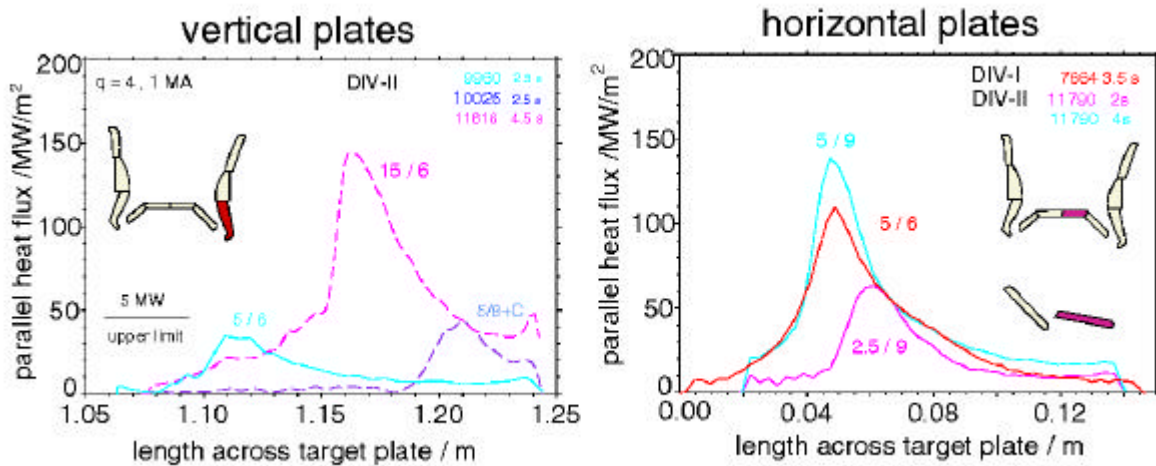


Figure 7. The maximum heat flux is reduced by about a factor of 2 in the closed Div-II compared to the open Div-I (ASDEX Upgrade). Heat flux values at the top of the roof baffle in Div-II are as high as in Div-I.

of advanced or optimised divertors have a higher divertor density, a good impurity retention, and show an increased helium compression compared to open divertor structures (Div I). The positive effect of a closed divertor structure on the reduction of the divertor heat load was e.g. demonstrated with the Lyra shaped Div II in ASDEX Upgrade and the MK-GB divertor at JET.

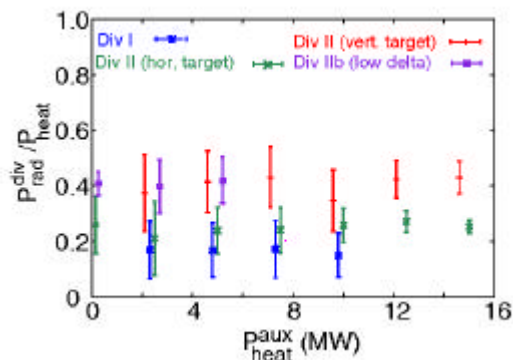


Figure 6. Divertor radiation (radiation below the x-point) for different divertor geometries. (ASDEX Upgrade).

this geometry is rather open. This kind of discharges show a radiation level comparable to the level of the open Div I, as it is expected. A detailed discussion of radiation levels and the power balance is given in [5], and of the different divertor loads in [6]. Due to the radiative volume in front of the target plates (Fig. 8) the divertor itself is loaded with a nearly homogeneous power density of about $100 \div 200 \text{ kW/m}^2$ [5,6].

The higher divertor radiation in Div II is a result of 3 processes: (i) the vertical orientation of the strike point module, which results in a preferential direction for sputtered and desorbed particles against the separatrix, increasing the effective particle density in the hot region near the separatrix. (ii) This region is cooled down by carbon radiation to a temperature of a few eV. (iii) At this temperatures radiation of hydrogen becomes significant [4,7] and increases the radiation losses further on. The serial action of both processes is necessary to explain the radiative losses in the divertor.

The change from the open divertor (Div I) to the closed divertor (Div II) results in a reduction of the maximum divertor load and an increase of the divertor radiation for comparable discharge conditions. Fig. 6 shows heat flux profiles measured by thermography in Div I and Div II. The reduction of maximum heat flux is partly attributed to the larger wetted area in Div II (see Fig. 3) but mostly to an increase of the radiation capability in the divertor region. The divertor radiation, i.e. the radiation below the x-point, is increased by about a factor of two compared to an open configuration (Div I) (Fig. 7). Running the strike point onto the vertical part of the roof baffle of Div II results in a decrease of the level of divertor radiation because

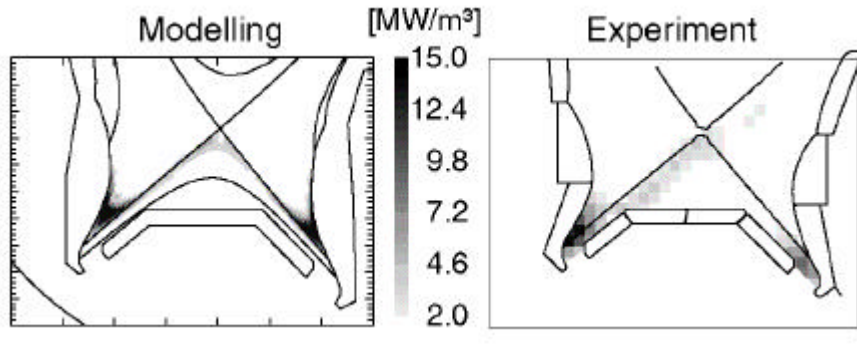


Figure 8. Radiation losses from B2-Eirene calculation (left) and derived from bolometric measurements (right). The spatial resolution of the bolometer system was increased by vertical strike point movement to detect the radiation band.

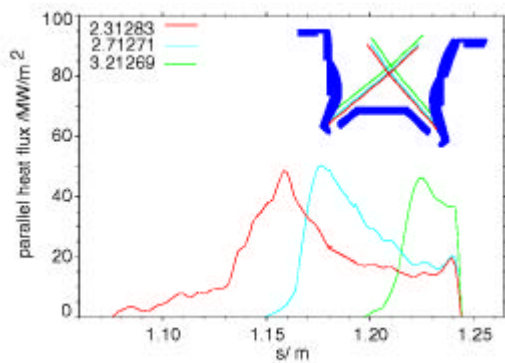


Figure 9. Parallel heat flux profiles at the outer target for different strike point positions in the divertor fan.

This is supported by extensive B2-EIRENE modelling of H-mode discharges with Div II configuration. The modelling ruled out that the radiation zone should be more narrower than deduced from bolometric measurements which are limited by the number and width of the viewing cords. To overcome this restriction special experiments were performed with a vertical movement of the strike zone position. The discharge parameters were kept constant. The existence of a narrow radiation pattern, as predicted by modelling could be verified experimentally [8].

The inner and outer strike points were moved from a position deep inside the divertor leg upwards into a region above the roof baffle. The corresponding parallel heat flux, shown in Fig. 8, show no significant change of the maximum heat flux. This indicates, that the heat flux to the target did not depend strongly on the tightness of the divertor leg, i.e. the existence of the roof baffle.

4.2. Profile shape

Because the maximum heat flux and not the total heat flux is a critical value for divertor design, the parameter dependence of the profile width is investigated at different experiments (JT 60 [9], AUG [10], DIII-D [11]). Different values for profile characterisation are proposed. The advantages and disadvantages of each characterisation parameter should not be discussed in this paper. At ASDEX Upgrade the profiles are characterised by fitting an e-folding length near to the maximum of the peak and measuring the peak width at half maximum in accordance with the ITER edge/divertor scalar database. The temporal evolution of peak heat flux and e-folding length into the SOL during a discharge with power ramp up is shown in Fig. 10. The measured decay length is nearly constant and the maximum heat flux increases proportional to the input power during the L-mode phase of the discharge. This behaviour changes during the H-mode phase where the decay length increases with heating power and the increase of the maximum heat flux is less pronounced. A detailed statistical analysis of about 50 H-mode discharges at moderate densities in Div I [10] results in the following scaling for the maximum heat flux and the decay length with the power crossing the separatrix, the line averaged density, and the safety factor:

$$q_{\max} (Wm^{-2}) = 8.837 \times 10^{13} P_{\text{Plate}}^{0.5 \pm 0.05} (W) q_{95}^{-0.27 \pm 0.3} \bar{n}_e^{-0.77 \pm 0.16} (10^{19} m^{-3})$$

$$l_p (mm) = 6.56 \times 10^{-3} P_{\text{Plate}}^{0.52 \pm 0.05} (W) q_{95}^{0.7 \pm 0.3} \bar{n}_e^{-0.09 \pm 0.17} (10^{19} m^{-3})$$

This scaling reveals that both the maximum heat flux and the decay length increase with the square root of the total power into the divertor, so that their product, which is proportional to the peak area, is kept nearly constant. The density effects the maximum heat flux, whereas the decay length

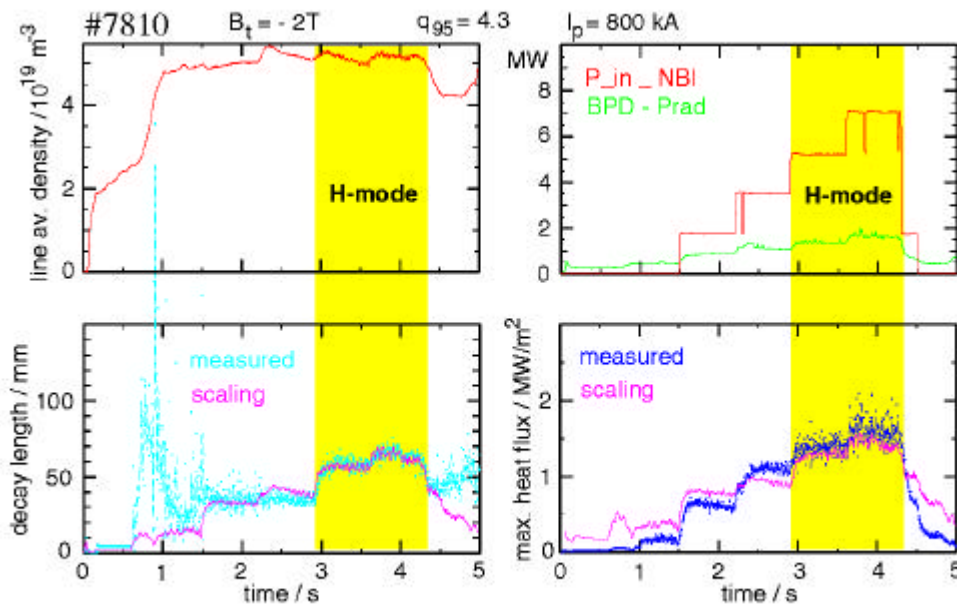


Figure 10. Change of the maximum heat flux and the decay length in the outer divertor (Div-I) of ASDEX Upgrade for L and H-mode type discharges. The H-mode scaling describes the behaviour in a single discharge.

behaviour is influenced by the safety factor. An increase of the line averaged density tends to increase the separatrix density and decreases the separatrix temperature. As a result the parallel heat flux to the target plates is reduced because electron heat conduction is the dominating transport mechanism. The safety factor is proportional to the connection length between midplane and target plate. An increasing connection length increases the time for perpendicular transport and broadens the profile.

A multi-machine scaling of the midplane heat flux decay length, using data from JT-60, AUG, DIII-D, and JET, is presented in [12]. For L-mode discharges the e-folding length, defined in this paper as total power to the plate divided by the maximum heat flux, increases weakly with the power to the divertor, $I_q^{L-1} \sim P_{div}^{-0.19 \pm 0.05}$. The H-mode scaling of data without gas puffing shows a positive dependence from the power to the divertor, $I_q^{H-1} \sim P_{div}^{0.44 \pm 0.04}$. Both scalings result in a positive dependence from the safety factor, q_{95} .

Recent results from JET, where thermographic measurements requires special shots with a separatrix position in the field of view of the IR camera, show no variation of the decay length with heating power but a strong increase with increasing safety factor. Target heat flux profiles derived from thermocouple measurements during special discharges with strike point movement results in a negative power dependence of the e-folding length from the power to the divertor [13, 14]. Scaling studies at DIII-D [15] gives a linear increase of the peak heat flux and the total power to the divertor with the input power. The analysis of profiles measured in Div II at ASDEX Upgrade could not be described with the Div-I scaling. This data show a linear dependence of the maximum heat flux from the divertor load and no dependence for the e-folding length [16].

The heat flux e-folding length (scrape off layer width) is analytically described by a competition of parallel and perpendicular transport so that, for a qualitative discussion, the characteristic thickness of the SOL can be described by [17]: $\Delta_s \sim (c_{\perp} t_{\parallel})^{1/2}$ where t_{\parallel} is the energy confinement time of the SOL given by the ratio of stored energy in the SOL and the power influx, P_{sep} , and c_{\perp} the

perpendicular transport coefficient. The SOL-width becomes than: $\Delta_q \sim \frac{n_s T_s}{P_{sep}} \mathbf{c}_\perp$. The SOL width

becomes broader with the electron pressure in the midplane and the perpendicular electron heat conductivity. It is steepened with power crossing the separatrix. In the case of an H-mode edge at the pressure limit, i.e. $n_s T_s = const.$, the width depends simply from the ratio of the perpendicular heat conduction and the power crossing the separatrix, which is linked to the electron temperature at the separatrix. To get a positive power law for the dependence of the SOL width from the power crossing the separatrix, the electron heat conductivity must increase more than linear with P_{sep} . If the plasma edge is not at the pressure limit, an increase of heating power can increase the edge pressure. This results in an surplus in peak broadening compared to pressure limit discharges and might explain the differences between the latest JET and DIII-D results and the scaling as well as the differences between Div I and Div II in ASDEX Upgrade.

4.3. Double null configurations

A further possibility to reduce the maximum heat flux and the total power to single divertor plates is to increase the wetted area and to distribute the heat flux to more than one divertor. The magnetic coil system of most of the tokamaks allow to run magnetic configurations with two xpoints and separatrices, respectively. The separatrix which limits the core plasma is the active separatrix. If the corresponding xpoint is below the plasma column the configuration is a lower single null (SNL) configuration and it is an upper single null configuration (SNU) in the opposite situation. In the limit, that both xpoints are active it is a double null (DN) configuration and the power crossing the separatrix can flow to the upper as well as the lower divertor plates. The operation around the double

null configuration was investigated at DIII-D [18,19] and at ASDEX Upgrade[20]. In this paper we will focus on the power deposition and not on the plasma performance which is also effected by the configuration change.

In the experiments performed, the distance between both separatrices was varied by changing slowly the configuration from SNL to SNU, crossing the double DN configuration and monitoring the power to the divertor plates by IR cameras. When the distance between both separatrices becomes comparable to the e-folding length of the heat flux in the midplane a significant part of the heat flows along the 'inactive' separatrix to the second divertor and reduces the heat load to the active one. The balance between both divertors is shown in dependence on the separatrix distance in the outer midplane of DIII-D in Fig. 11. The load change for the attached (high heat flux) situation is between ± 1 cm separatrix distance as expected from a few millimetre heat flux decay length. The balanced situation is about 2mm away from the DN configuration. This sharp change in divertor load requires a sophisticated plasma control system keeping the plasma configuration constant within a few millimetre.

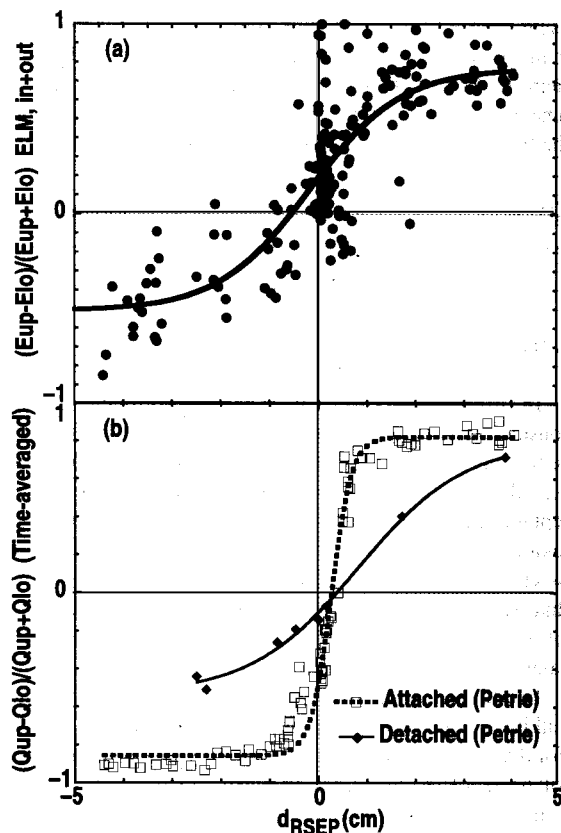


Figure 11. Redistributon of divertor heat load for a change between SNL and SNU configuration.

The energy deposition due to ELMs show a significant smoother change of the power load. The redistribution pattern is about a factor of four broader than the time averaged values [19]. This mitigates the necessity for accurate position control.

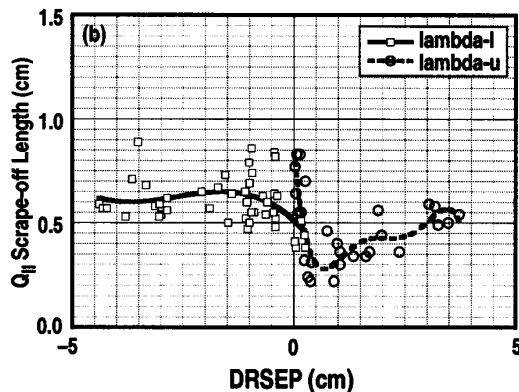


Figure 12. The e-folding length becomes shorter near to the double null configuration.

the midplane e-folding length of the heat flux show the decrease of the total and the maximum power to the lower outer divertor plate [20]. But the ELM averaged profiles show now significant change of the e-folding length with the separatrix distance.

Discharges with double null divertor configuration are one way to decrease the averaged load to a divertor plate. It requires the installation of a second divertor and a appropriate configuration control system.

4.4. Asymmetry and detachment

The power flowing from the plasma column into the SOL is not equally distributed between the inner and outer divertor plate. An asymmetry ratio of the target load onto the inner and outer divertor is measured with cooling water calorimetry, thermography, and Langmuir probes. An outer/inner ratio of 2-3 is reported from AUG [20], DIII-D [19], and Alcator C-Mod [22] for an $ion - \nabla \bar{B}$ drift direction towards the x-point. A reversal of the magnetic field direction - $ion - \nabla \bar{B}$ drift direction away from the x-point - can partly reduce this asymmetry but did not result in a reversal of the in/out ratio [20, 22].

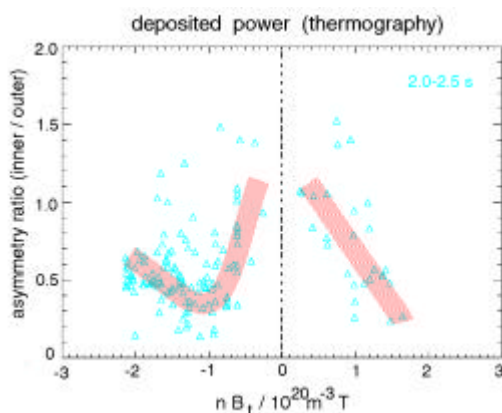


Figure 13. Change of the in/out asymmetry for both ion-gradB drift directions in ASDEX Upgrade with line averaged density.

Because the maximum heat flux is the critical value it is essential to reduce the maximum heat flux and not only the total power to the divertor. This requires that the profile shape is kept constant or becomes broader with decreasing separatrix distance. Fig. 12 shows the heat flux e-folding length for the profiles in the upper and lower divertor. It is obvious that near to the symmetry point (DN) the profile becomes steeper and that the e-folding length is shorter in the upper divertor. So that the reduction of the maximum heat flux in the case of symmetric power distribution between upper and lower divertor is less than the possible factor of two.

The experiment performed at ASDEX to measure

the experiment performed at ASDEX to measure the measurements show that the in/out ratio varies strongly with the line averaged density. With increasing density the in/out ratio goes down from 1 (symmetry) to values of about 0.5. due to a reduction of the heat flux onto the inner divertor. With increasing density the asymmetry becomes more symmetric because than the outer divertor starts to detach.

In simplest 1D models the symmetry of heat deposition to the divertor plates is spontaneous broken with equal probability of either direction for in/out asymmetry when the radiation fraction exceeds a critical value [23]. Detailed B2-Eirene modelling predicts that this equal probability for symmetry braking does not hold under experimental conditions due to the outboard dominance of the thermal transport

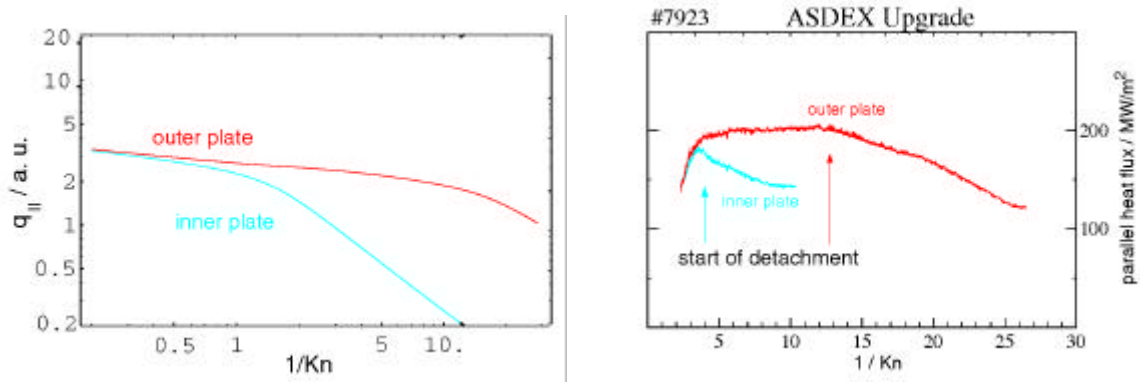


Figure 14. Change of the heat flux with inverse Knudsen number as predicted from a simple model (left) and measured by thermography (right).

in the core which results in a longer path into the inner leg [24]. This is consistent with an in/out asymmetry independent from the orientation of the ion-gradB drift direction.

The detachment behaviour of the divertor in dependence from the SOL collisionality was investigated by varying the flux tube length in the SOL, keeping the hydrogen density constant at $\bar{n}_e = 6 \times 10^{19} \text{ m}^{-3}$. The flux tube length was increased by ramping down the plasma current from $I_p = 1.2 \text{ MA}$ to $I_p = 0.6 \text{ MA}$ which results in an increase of the safety factor q_5 from 3 to 7. The L-mode discharge in hydrogen was additionally heated with 3.7 MW NBI power. The collisionality is expressed as Knudsen number $K_N = \mathbf{I}_{ee,m} / L_{||,o}$, i.e. the ratio of the mean free path for electron-electron collisions, $\mathbf{I}_{ee,m}$, and the connection length – midplane to outer plate, $L_{||,o}$. The experimental result was compared to a simple 1D fluid model [25]. The model assumes non-ambipolar boundary conditions at the target resulting in a current flow through the SOL. The connection lengths between midplane and each target are allowed to be asymmetric. The model ignores radiation, ionisation and charge exchange. The model predicts a decreasing target load with inverse Knudsen number (Fig. 14a), either on account of increasing electron-electron collisions or by increasing the connection lengths. A strong decrease of the target load is expected if the mean free path of the electrons is only a fraction of the connection length, $K_n < 0.1$.

The experimental result is shown in Fig.14. The power load starts to decrease at a inverse Knudsen number of about 10 as predicted by the model. The inner divertor detaches first due to the longer connection length. The Knudsen number at the beginning of the detachment for both divertors reflects the ratio of the detection lengths.

4.5. Comparison of profile measurement

Measurements of the divertor power load are performed with different diagnostics. The energy to the divertor is measured by cooling water calorimetry or thermometry. Time resolved heat flux data are derived from Langmuir probe measurements or from the surface temperature evolution as measured with IR cameras. The heat flux is then calculated by solving the heat conduction equation with the measured temperature as edge condition (thermography). Thermography measures the net power deposition to the target, whereas Langmuir probes measures the ion saturation current and the electron temperature. From this data the heat flux to the target is calculated making assumptions on the ratio of electron and ion temperature as well as on the electrical sheath in front of the target.

Moving the separatrix across the target plates avoids the problem of the relatively big distances between Langmuir tips, compared to the decay length, and gives the opportunity to measure heat flux profiles across the plates which can be compared with that, measured themographically (Fig. 15). The ratio is about 1.5 at the separatrix and decreases slowly with the distance from the separatrix. Fig. (16) shows the ratio for a set of 37 ohmic and L-mode discharges. A ratio of unity away from the separatrix indicates that most of the power is deposited by charged particles. Close to the separatrix the ratio

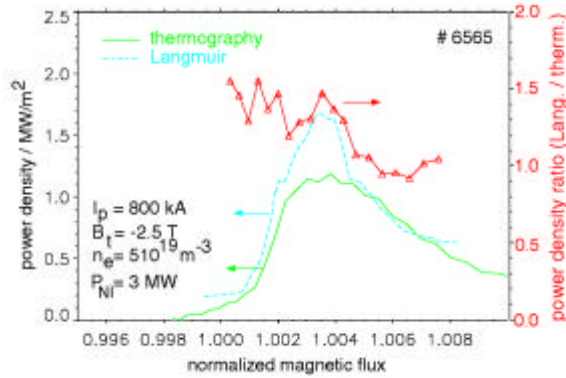


Figure 15. Heat flux profiles measured at the outer target by thermography and Langmuir probes mapped to normalized magnetic flux coordinates. The difference between both measurements decreases with the distance from the separatrix.

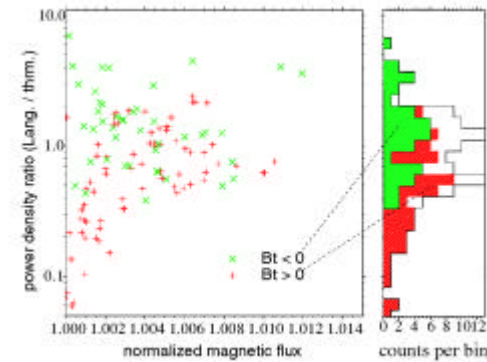


Figure 16. Heat flux ratio Langmuir/thermography for 37 ohmic and L-mode discharges and both direction of magnetic field.

depends on the field direction. It is about 3 in the case of normal field direction and is 1/3 for reversed field. Phenomenological, this effect is due to a different behaviour of the temperature and density profiles, as measured with Langmuir probes, for both direction of the magnetic field. In the case of normal field direction, the maximum of temperature and density profile is at the same location. For the reversed field direction the temperature peak is moved away from the density peak into the direction of the private flux region [21].

Thermographic measurements are independent from the direction of the magnetic field, whereas electrical measurements might be influenced by strong radial electrical fields near to the separatrix, particularly if the radial dimension of the probes becomes comparable to the gradients of radial electrical fields.

5. Pulsed heat load

In addition to the stationary divertor load, burst like heat flux arrives the target during nearly all kind of plasma confinement regimes. There are different physical reason for such events. Sawtooth instabilities transport core energy to the edge which results in a decrease of the plasma stored energy by a few per cent and a negligible increase of the target load.

High confinement regimes are accompanied by edge localised modes (ELMs). Each ELM expels energy from the plasma edge on a microsecond time scale which is then transported to the plates. The amount of energy and the time scale of energy deposition depends on the type of the instability. It exists different types of ELMs. The most energetic ELMs are type-III and type-I ELMs. They are distinguished by the power dependence of the ELM frequency, f_{ELM} . The change of the ELM frequency with heating power and otherwise constant plasma parameters, $\frac{df_{ELM}}{dP_{heat}}$, is negative for type-III ELMs and it is positive for type-I ELMs [26].

Each change of energy confinement in the plasma, e.g by L-H mode change or by a loss of the internal transport barrier results in a change of plasma stored energy which modifies the power crossing the separatrix on a time scale of the energy confinement time.

Only disruptions and type-I ELMs are violating the energy impact limit, as given by the material parameters (table I). Unfortunately, the H-mode confinement, as presently envisaged as operating regime for ITER, is connected with type-I ELMs. Mitigating the energy impact to the target without deterioration of plasma performance is a main aim of ELM investigation. In this chapter the amount of ELM energy, the deposition pattern, and the temporal behaviour of type-I ELMs will be discussed.

The present understanding of the mechanism of energy exhaust from the plasma edge during type-I ELMs is that the plasma edge pressure is near to the ballooning limit and then a peeling mode is triggered which intermix the outer field lines and increases the perpendicular energy transport across the separatrix. Experimentally, the strength of ELMs is deduced from the loss in stored plasma energy, ΔW_{Mhd} , and from target heat flux measurements by Langmuir probes and thermography. A detailed analysis of particle and temperature loss is performed by using edge electron temperature and density profiles.

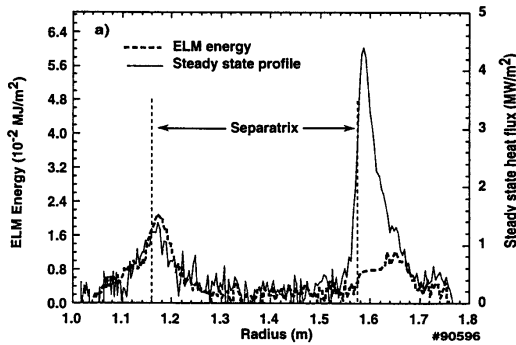


Figure 17. Heat flux deposition pattern measured in DIII-D. The in/out asymmetry is inverted during the ELM.

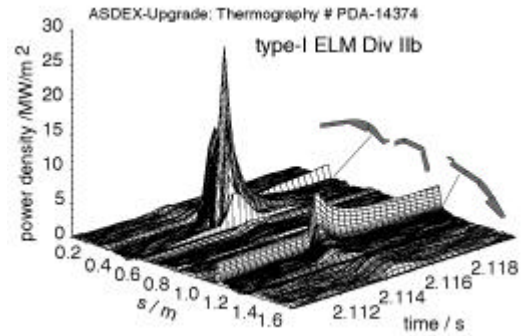


Figure 18. Heat flux deposition pattern measured in ASDEX Upgrade. The in/out asymmetry is inverted during the ELM.

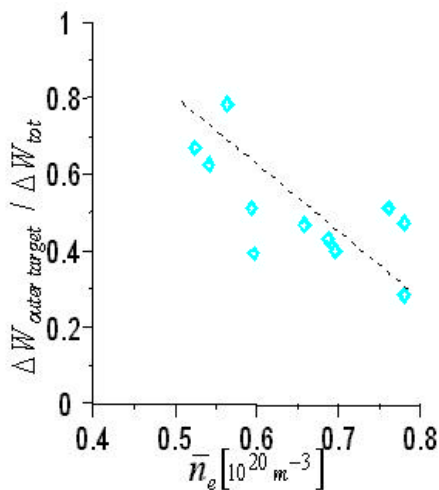


Figure 19. The fraction of ELM energy loss deposited at the outer target plate decreases with increasing line averaged density.

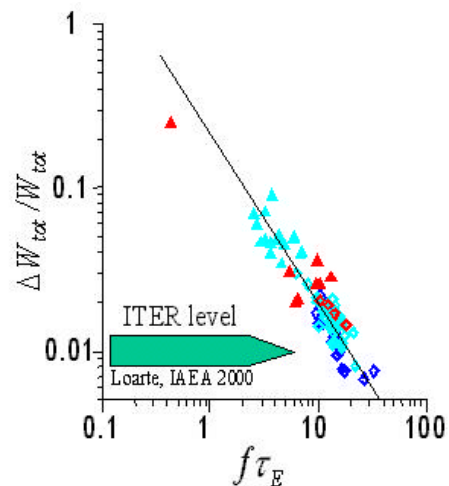


Figure 20. ELM energy loss in JET and ASDEX Upgrade vs the normalised ELM frequency. The ITER level required to stay below the energy impact limit is indicated.

Typical heat flux deposition pattern as measured at DIII-D and ASDEX Upgrade are shown in Fig. (17) and Fig. (18), respectively. The asymmetry between in/out power load is reversed from about 0.5 to 2 during type-I ELMs as compared to averaged or in between ELM conditions. An in/out ratio of about unity is reported from JET [30], where most of the power is deposited to the outer plate in between ELMs with an asymmetry ratio in/out of about 0.5. The ELM transported power, $\frac{\Delta W_{\text{ELM}} f_{\text{ELM}}}{P_{\text{heat}}}$, is between 20 and 30 % at JET, DIII-D, and ASDEX Upgrade [31]. The fraction of stored energy lost with an ELM depends on the edge plasma conditions. With increasing density the ELM energy loss decreases (Fig. 19). Because edge parameters and plasma confinement are not independent from each other the fractional energy loss of a type-I ELM is shown in Fig. 20 vs. the dimensionless parameter $f_{\text{ELM}} \times \tau_E$ for JET and ASDEX Upgrade data.

The variation of ELM heat flux profiles and of the temporal behaviour of the power deposition is high in type-I H-mode discharges at Jet and less pronounced at ASDEX Upgrade and DIII-D. The maximum of the divertor heat load jumps a few centimetre away from the separatrix during ELMs in hot ion H-mode discharges, whereas regular H mode discharges with type-III and type-I didn't show this behaviour [30,13]. The maximum of the power deposition during the ELM is at the same divertor

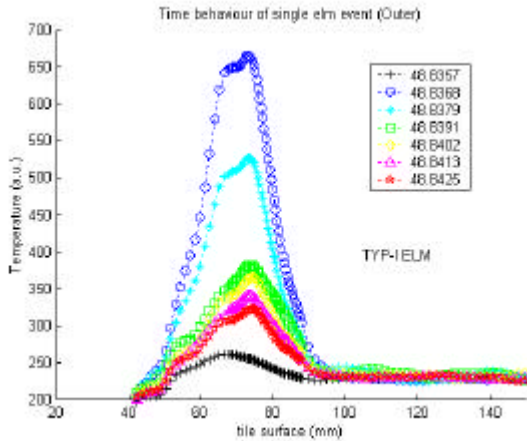


Figure 21 Temporal behaviour of surface temperature during a type-I ELM at the outer plate of JET.

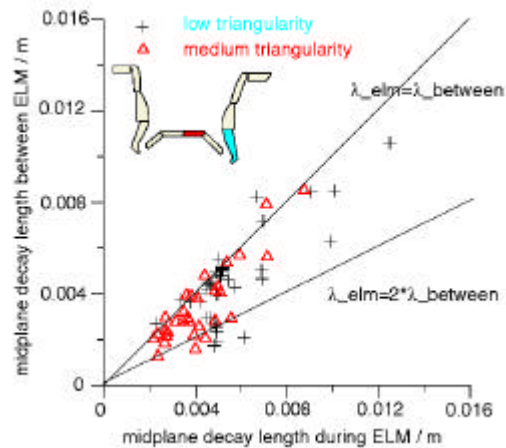


Figure 22 Heat flux decay length in the outer midplane of ASDEX Upgrade during and between type-I ELMs.

position as in between the ELM (21). This behaviour is also found at ASDEX Upgrade and DIII-D. The shape of the profile itself is not changed significantly during the ELM (Fig 21) and Fig. (22) so that the ELM effect on the profile is simply a scaling with a factor between 1.5 and 5. The ELM behaviour at the inner plate show a pronounced peak near to the separatrix with an e-folding length comparable to that at the outer plate. The profile shape during an ELM is not significantly broadened at JET, ASDEX Upgrade and DIII-D. This means that ELM mitigating due to profile broadening is no significant effect. Profile stiffness in terms of transport means that the ratio of parallel to perpendicular transport is kept constant. The reason for the change of the asymmetry ratio during the ELM is an open question, but it helps to equalise the power load between inner and outer divertor.

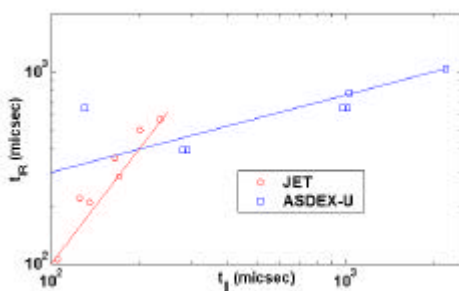


Figure 23. The parallel transport time shows a linear correlation to the characteristic energy deposition time as found by IR-thermography for ASDEX-Upgrade and JET.

A physical model of the empirical description is given in [29].

With increasing parallel energy transport time the ELM rise time increases mitigating the energy impact, as it is shown in Fig. 23. With increasing density the ELM losses itself becomes smaller further reducing the ELM energy. Nevertheless, the expected ELM impact is higher the tolerable value.

Whether or not the ELMs becomes shorter with machine size is essential to predict the ELM load to the ITER divertor. Typical heat flux rise times at the outer target plate defined as the increase from the inter ELM value to the ELM maximum is in between 260 μ s and 1 ms at ASDEX Upgrade and varies between (100 and 400) μ s at JET. The temporal decay can be described by an e-folding length of about 1 ms for both machines [32,33]. The energy flow from the midplane to the separatrix is described by empirical and semi-empirical models [27,28], which explain the experimental result, that the amount of energy lost by an ELM depends on the ratio of ELM duration and parallel transport time as

A loophole from this dilemma is to develop discharge scenarios with high confinement and small ELMs as it was found at DIII-D, and ASDEX Upgrade. Discharges with high confinement at high density and a beta normalized of 3.5 were recently established [34]. Up to now the operation regime is restricted to q_5 values larger than 3.5, and plasma configurations near double null. There is no clear change between type-I and type-II (ore grassy) ELMs. But also the type-I ELMs are smaller and becomes tolerable.

6. Summary

There are two critical parameter for heat load deposition in the divertor. The maximum stationary heat load which can be handled by the divertor structure is limited to $10 \div 15 \text{ MW} / \text{m}^2$ for present designs of actively cooled divertors. Pulsed heat loads result in a fast increase of the surface temperature. The sublimation or melting temperature of the target material determines the tolerable heat impact to $\Delta W / \sqrt{t} < 20 \div 40 \text{ MW} \sqrt{s} / \text{m}^2$ for carbon and tungsten, respectively.

The stationary power load to the divertor can be reduced by an optimised divertor configuration which makes use from the flux expansion and from the increased radiation capability of a closed divertor structure.

The change of the heat flux profile shape with heating power is not predictable from present experiments. Data from Div-I in ASDEX Upgrade and a multi machine scaling points on an increase of the heat flux decay length with increasing power. The maximum heat flux increases less than linear ($P^{0.4-0.5}$). Recent experiments with high confinement H-modes reveals a linear dependence of the maximum heat flux from the heating power. Thermocouple experiments at JET show a steepening of the decay length with heating power.

The beneficial effect of a doubled area for power deposition in double null configurations is partly compensated by a steepening of the profile.

The stationary heat load is asymmetric distributed between the inner and outer divertor. The in/out asymmetry ratio is about 0.5. This ratio is reversed during type-I Elms in DIII-D and ASDEX Upgrade. It is unity in JET.

The ELM transported power is between 10 and 30%. The fraction of energy loss per ELM decreases with the product of frequency and energy confinement time.

The heat flux profile is not broadened significantly during a type-I ELM and the ELM rise time depends on the parallel energy transport time.

The extrapolation of the maximum stationary heat flux to ITER conditions depends on the extrapolation of the profile shape. Assuming a linear increase with heating power and fixed e-folding length, the expected peak value can be tolerated. Whereas the type ELM energy impact is higher the limit.

Discharge scenarios with reduced ELM size (type-II) keeping the type-I H mode confinement are a loophole.

7. References

- [1] ASDEX team, Nucl. Fusion **29** (1989) 1949
- [2] G A0 FDR 3 01-05-18 R 0.1 (Summary of the ITER final design report , May 2001)
- [3] H. Greuner et al., Proc of the 20th SOFT, Marseille (1998), Vol.1, 249
- [4] A. Kallenbach, et al., Nucl. Fusion **39** (1999) 901.
- [5] J.C. Fuchs, et al., J. Nucl. Mater. 290-293 (2001) 529
- [6] A. Herrmann, et al., J. Nucl. Mater. 266-269 (1999) 291
- [7] Divertor modelling
- [8] J.C. Fuchs, et al., (Proc. 25th Eur. Conf., Praha, 1998), Vol. 22C, (1998) 1510

- [9] K. Itami, et al., Plasma Physics and Controlled Nuclear Fusion Research (Proc. 14th Int. Conf. Würzburg, 1992) Vol. 1 IAEA (1993) 391
- [10] A. Herrmann, et al., Controlled Fusion and Plasma Physics (Proc. 23rd Eur. Conf., Kiev, 1996), Vol. 20C, Part II (1996) 807
- [11] DIII-D - Scaling
- [12] A. Loarte, et al., J. Nucl. Mater. 266-269 (1999) 587
- [13] G. Mathews, et. al., J. Nucl. Mater. 290-293 (2001) 668
- [14] W. Fundamesni, et al., Controlled Fusion and Plasma Physics (Proc. 28th Eur. Conf., Madeira, 2001)
- [15] C.L. Lasnier, et al., Nucl. Fusion **38**(1998)1225
- [16] A. Herrmann, et al., Controlled Fusion and Plasma Physics (Proc. 25th Eur. Conf., Praha, 1998), Vol. 22C, (1998) 488
- [17] P.J. Harbour, Nucl. Fusion **24**(1984)1211
- [18] Petri, et al., Controlled Fusion and Plasma Physics (Proc. 26th Eur. Conf., Maastricht, 1999), Vol. 23J (1999) 1237
- [19] C.J. Lasnier, et al., J. Nucl. Mater. 290-293 (2001) 1093
- [20] A. Herrmann, et al., J. Nucl. Mater. 290-293 (2001) 619
- [21] M. Laux, et al., Controlled Fusion and Plasma Physics (Proc. 22nd Eur. Conf., Bornemouth, 1995), Vol 19C Part III (1995) 097
- [22] I. Hutchinson, et al., Plasma Phys. Controlled Fusion **37** (1995) 1389
- [23] G.M. Staebler, Nucl. Fusion **36** (1996) 1437
- [24] U. Wenzel, et al., Nucl. Fusion – submitted
- [25] P. J. Harbour, Contrb. Plasma Phys. 28 (1988) 4/5 417-419
- [26] H. Zohm, Plasma Phys. Control. Fusion **38** (1996) 105
- [27] G. Janeschitz, et al., J. Nucl. Mater. 290-293 (2001) 1
- [28] A. Loarte, et al., 18th IAEA Sorento, 2000
- [29] Yu. Igitkhanov, et al., Controlled Fusion and Plasma Physics (Proc. 28th Eur. Conf., Madeira, 2001)
- [30] T. Eich, et al., Controlled Fusion and Plasma Physics (Proc. 28th Eur. Conf., Madeira, 2001)
- [31] A.W. Leonard, J. Nucl. Mater. 266-269 (1999) 109
- [32] M. Laux, et al., Controlled Fusion and Plasma Physics (Proc. 28th Eur. Conf., Madeira, 2001)
- [33] S. Jachmich, et al., Controlled Fusion and Plasma Physics (Proc. 28th Eur. Conf., Madeira, 2001)
- [34] J. Stober, et al., Controlled Fusion and Plasma Physics (Proc. 28th Eur. Conf., Madeira, 2001)

8. Figure captions

1. Magnetic configuration for a lower single null plasma configuration. The midplane distance of magnetic flux surfaces is 1 cm. The separatrix distance (active to inactive) is 1.5 cm in the midplane.
2. Divertor geometries investigated in ASDEX Upgrade (top) and corresponding pitch ratios (bottom).
3. The length of the flux tube connecting outer midplane and outer divertor decreases with the distance from the separatrix.
4. Dependence of the divertor and separatrix density on the neutral gas flux density for low and high recycling SOL-regime in ohmic discharges (ASDEX Upgrade).
5. Radiation loss function for carbon as a function of electron temperature (D. Post)

6. The maximum heat flux is reduced by about a factor of 2 in the closed Div-II compared to the open Div-I (ASDEX Upgrade). Heat flux values at the top of the roof baffle in Div-II are as high as in Div-I.
7. Divertor radiation (radiation below the x-point) for different divertor geometries.
8. Radiation losses from B2-Eirene calculation (left) and derived from bolometric measurements (right). The spatial resolution of the bolometer system was increased by vertical strike point movement to detect the radiation band.
9. Parallel heat flux profiles at the outer target for different strike point positions in the divertor fan.
10. Change of the maximum heat flux and the decay length in the outer divertor (Div-I) of ASDEX Upgrade for L and H-mode type discharges. The H-mode scaling describes the behaviour in a single discharge.
11. Redistribution of divertor heat load for a change between SNL and SNU configuration.
12. The e-folding length becomes shorter near to the double null configuration.
13. Change of the in/out asymmetry for both ion-gradB drift directions in ASDEX Upgrade with line averaged density.
14. Change of the heat flux with inverse Knudsen number as predicted from a simple model (left) and measured by thermography (right).
15. Heat flux profiles measured at the outer target by thermography and Langmuir probes mapped to normalized magnetic flux coordinates. The difference between both measurements decreases with the distance from the separatrix.
16. Heat flux ratio Langmuir/thermography for 37 ohmic and L-mode discharges and both direction of magnetic field.
17. Heat flux deposition pattern measured in DIII-D. The in/out asymmetry is inversed during the ELM.
18. Heat flux deposition pattern measured in ASDEX Upgrade. The in/out asymmetry is inversed during the ELM.
19. The fraction of ELM energy loss deposited at the outer target plate decreases with increasing line averaged density.
20. ELM energy loss in JET and ASDEX Upgrade vs the normalised ELM frequency. The ITER level required to stay below the energy impact limit is indicated.
21. Temporal behaviour of surface temperature during a type-I ELM at the outer plate of JET.
22. Heat flux decay length in the outer midplane of ASDEX Upgrade during and between type-I ELMs.
23. The parallel transport time shows a linear correlation to the characteristic energy deposition time as found by IR-thermography for ASDEX-Upgrade and JET.